ICF100217OR

MICROELECTROMECHANICAL STRUCTURES FOR MULTIAXIAL FATIGUE TESTING

K. Komvopoulos

Department of Mechanical Engineering, University of California, Berkeley, CA 94720, USA

ABSTRACT

Recent advances in micromachine devices have increased the need for information about the dynamic material behavior at scales relevant to microelectromechanical systems (MEMS). However, the present understanding of fatigue at MEMS scales is relatively sparse. The review of the literature indicates that there is a significant scatter in the fatigue strength of silicon, the basic structural material of MEMS. In addition, most of the previous work has been performed with very simple devices that do not simulate fatigue under multiaxial loading conditions, similar to those occurring during micromachine operation. The aim of this publication, therefore, is to introduce novel microstructures, fabricated by standard surface micromachining, that enable fatigue testing under conditions typical of most MEMS devices. Cyclic loading is generated by interdigitized comb drives, arranged along radial "spokes" extending from a suspended ring held in place by thin flexures (fatigue specimens) attached to an anchor at the center of the device. The test structures are excited at resonance using on-chip actuation to generate the forces required to produce fatigue damage. The fabrication process for obtaining such microstructures and preliminary results from fatigue experiments performed at atmospheric conditions are presented and discussed in the context of damage accumulation in polycrystalline silicon microstructures subjected to cyclic loading.

KEYWORDS

Microelectromechanical Systems (MEMS), Multi-axial loading, Fatigue, Damage

INTRODUCTION

Monitoring the movement, position, actuation, and signaling of microelectromechanical systems (MEMS) has been increasingly used to sense chemical, electrical, mechanical, and thermal processes. Developments in this emerging field have been based on a technological basis derived from the integrated circuitry industry and have led to the design, fabrication, and implementation of microsystems spanning a wide range of industrial and medical applications [1,2]. With an estimated compound annual growth rate of 50%, predictions suggest that MEMS device revenues will exceed approximately US$10 billion in the near future. Due to increasing demands for versatile microsystems, dramatic changes have been encountered in fabrication techniques, materials, and device dimensions, with ultimate goal to enhance micromachine sensitivity and endurance. Despite early indications suggesting that significant

opportunities exist for MEMS, a large number of challenging issues presently inhibit rapid evolution of micromachines from the laboratory to the application world. For such small devices, a number of physical effects have a different significance at the micrometer scale than at macroscopic scales. Consequently, the identification of the effects of process parameters on the microstructure and material behavior at the microscale and the development of testing methods yielding information about micromachine performance over a wide range of application conditions are of scientific and industrial significance.

The mechanical behavior of polycrystalline silicon (polysilicon) has attracted significant attention since it is considered to be the building block of integrated circuitry technology. However, most of the research has been concentrated on the static fracture strength of polysilicon. Greek and Johansson [3] performed a Weibull analysis and found polysilicon fracture strength between 1.0 and 1.25 GPa for tension loading. Sharpe et al. [4] used laser interferometry to measure the strain in microfabricated tensile specimens and determined a tensile strength of about 1.2 GPa. Koskinen et al. [5] performed tensile tests on polysilicon samples of varying grain size and measured fracture strength in the range of 2.86-3.37 GPa. Kapels et al. [6] tested 4 μm thick polysilicon structures and reported fracture strength values of approximately 3.4 and 2.9 GPa for bending and tension loading, respectively. Kahn et al. [7] used a probe tip to separate the end tips of a deeply notched cantilever specimen, and based on the stress at the crack tip (determined from the probe tip position at the instant of fracture) they found the fracture toughness to be equal to 2.3 $MPa \cdot m^{1/2}$, independent of specimen thickness and doping. Tsuchiya et al. [8] reported that the fracture strength of polysilicon crystallized from amorphous silicon is in the range of 2.0-2.7 GPa and decreases with increasing specimen length, whereas the effect of the specimen width is insignificant. It was observed that fracture initiated mostly from defects produced from sacrificial HF wet etching on the side surface and edge of the specimen and argued about the fracture dependence on surface defect density and the independence of fracture on the volumetric defect density. However, a comparison of the data given in some of the previous studies shows that the two lowest tensile strength values correspond to the specimens with the largest widths. Fracture of flexure elements due to the combined effects of tensile and bending cyclic stresses may exhibit a dependence on specimen width, and thus the conclusion drawn by Tsuchiya et al. [8] might not be applicable to different types of loading. Furthermore, even though in-plane tensile loading may be appropriate for devices having a thin membrane in tension (e.g., pressure sensors and strain gages), load bearing elements in most MEMS devices (e.g., accelerometers and actuators) are flexure systems usually subjected to in-plane bending, similar to the conditions in the tests performed by Jones at al. [9], Connally and Brown [10], and Van Arsdell and Brown [11].

From the above discussion, it is evident that new testing devices and methods are needed to reliably evaluate the micromechanical properties and dynamic performance of thin-film microstructures. The objective of this research, therefore, was the establishment of a standard methodology for mechanical property testing at the microscale using thin-film microstructures fabricated by surface micromachining. Preliminary results are presented to demonstrate the initial development of fatigue damage in polysilicon microstructures subjected to cyclic loading under ambient conditions.

EXPERIMENTAL

Significant errors in force measurements are often encountered with probe tips or load cells used to apply forces on microfabricated test specimens used for mechanical property characterization. This is mainly due to the difficulty to accurately determine the microscopic displacement of a macroscopic device. Hence, it is more advantageous to use on-chip electrostatic actuation generated from inderdigitized comb drives [10,11. This method of actuation was adopted in the design of the fatigue devices of this work.

Basic Characteristics of Fatigue Microstructures

The mask design and process flow were designed to allow some control over the dimensions of the test specimens. The height of the beams was controlled by the amount of a single polysilicon deposition and the width of the beams was defined by the anisotropic etch of the polysilicon with an oxide mask. A schematic of a microstructure for fatigue testing is shown in Fig. 1. The main design features of this design are summarized below.

(a) On-chip actuation by comb drives is used to generate an electrostatic force to fatigue the test specimen. This approach is superior to the charged parallel-plate method because the force produced is independent of position.

(b) Cyclic loading is generated by interdigitized comb drives arranged along radial “spokes” extending from a suspended ring held in place by thin flexure beams (fatigue specimens) that are attached to an anchor at the center of the device. Two fatigue specimens can be seen in Fig. 1.

(c) Movement is obtained by applying a potential difference between the suspended and stationary comb teeth using an electrical connection made to the specimen. Both test specimens were charged such that current flows no matter which one fractures. In addition to the bending stress, axial and transverse forces are exerted to the fatigue specimens by the rotating ring, leading to multi-axial loading conditions. This is a unique feature of the present design compared to previous similar devices [10,11].

(d) A vernier is used to estimate the rotation of the ring during actuation. A matching set of stationary indicator marks was placed near the end to allow measurement of angular displacements as small as 0.2^o, in order to correlate the movement and, in turn, the stress (or strain) amplitude due to the applied voltage, and to determine whether the compliance of the test specimens changed during testing. Since measurable displacements can only be obtained under dynamic conditions, determination of the maximum deflection based on the blurred edge of the resonating microstructure is approximate.

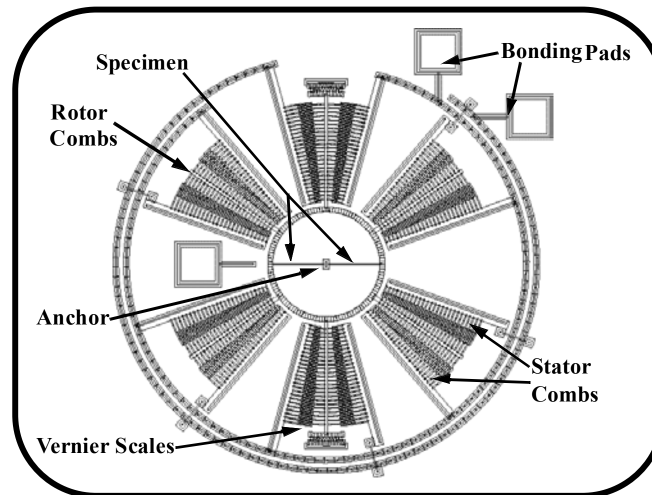

Figure 1: Schematic of fatigue test microstructure with two flexure beams (fatigue specimens).

Fatigue Microstructures

The fatigue specimens were excited at resonance by a sinusoidal electrostatic force generated by the rotary actuators. The evolution of fatigue damage was studied by observing the time it takes for the stiffness to decrease or equivalently the resonant frequency to change. The spring constant was determined based on Rayleigh’s method. This involved equating the potential energy of the flexures at their extreme positions to the sum of the kinetic energy of the flexures and the rotational kinetic energy of the actuator. Thus, the natural frequency of the system was monitored, and any deterioration (aside from drift effects) was attributed to fatigue damage accumulation in the flexure beams. The strain amplitude was determined from the specimen rotation (between 0.5^o and 3.5^o). To maintain the fatigue test structure at resonance, the natural frequency and amplitude must be controlled and tracked continuously over the range of anticipated frequency shifts. A phase detector can be used to measure the difference in phase between the driving

voltage applied to the forcing electrode and the output voltage of the sensor. Implementation of such control system requires circuitry that can sense motion based on the change of the system's capacitance, determine if the device is at resonance, and accordingly correct the driving frequency [12].

Fabrication Process

The fabrication process comprised doping a 100 μm thick p-type silicon wafer of 1-2 Ω·cm resistivity with phosphorus in a standard diffusion furnace using $POCl_3$ as the dopant source in order to prevent the occurrence of feed through charges to the substrate from the electrostatic devices on the surface. A 0.3 μm thick thermal oxide layer (1050°C) and a 0.6 μm low-stress LPCVD silicon nitride layer (835°C) were then deposited to produce an electrical isolation layer. This was followed by the deposition of a 0.5 μm LPCVD polysilicon film, which was patterned to obtain the anchor at the center of the structure. Subsequently, a 2 μm thick PSG sacrificial layer was deposited by LPCVD and annealed at 1050°C for 1 h in N_2. This sacrificial layer was patterned lithographically, and the anchors were transferred into the sacrificial PSG layer by plasma etching. The structural layer was deposited to a thickness of 2 μm. Then, the structural layer was coated with a thin (0.2 μm) PSG layer, and the wafer was annealed at 1050°C for 1 h. The anneal dopes the polysilicon with phosphorus from the PSG layers above and below it and also reduces the residual stress. The polysilicon and PSG masking layer were patterned using a mask designed to form the structural layer. The PSG layer was etched to produce a hard mask for subsequent polysilicon etch. After etching the polysilicon, the photoresist was stripped off and the remaining oxide hard mask was removed by plasma etching. Finally, diced wafers were immersed in a bath of 49% HF at room temperature for ~1.5 min, rinsed with DI water and methyl alcohol for several minutes, and successfully released by CO_2 supercritical drying performed at ~40 ^{o}C under pressure of ~1350 psi for 10 min. Figure 2 shows a scanning electron micrograph of a microdevice with two flexure (fatigue) specimens fixed to an anchor at the center of the device and an inner ring that can be rotated by the attached comb drives.

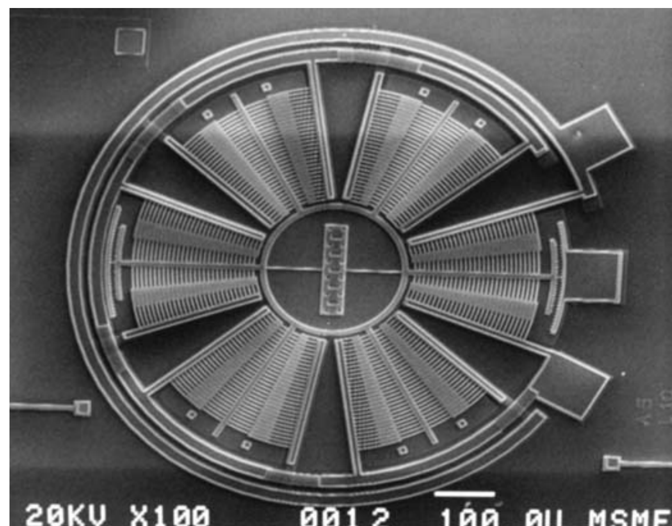

Figure 2: Scanning electron micrograph of a released microstructure with two flexure (fatigue) beams.

RESULTS AND DISCUSSION

From a dynamic analysis, the resonance frequency of the in-plane rotation of the specimens was predicted to be in the range of 8-60 kHz, depending of the number, length, and width of flexure beams. Figure 3 shows vibration results obtained from an experiment performed at atmospheric conditions with a microstructure having two flexure beams of 2 μm thickness, 4 μm width, and 100 μm length excited at different frequencies by an in-plane driving force. The motion of the oscillating device was captured by a

strobe-like system. The displacement was determined by a motion detection technique of image processing. The frequency response of the device was obtained by frequency sweeping. Sixteen frequency points specified in a certain range around the natural frequency were swept one by one and the amplitude and phase of the oscillation at each frequency was measured. To determine the resonant frequency more accurately, a second measurement was performed and the frequency points were specified in such a way that the points were denser close to the resonant frequency and sparser away from the resonant frequency. The results for the amplitude of the displacement and the phase shift, shown in Figs. 3(a) and 3(b), respectively, indicate that the resonance frequency of the in-plane rotation is equal to 14.2 kHz. Considering the unknown damping characteristics of the system, the measured resonance frequency is in close agreement with the value of 15.5 kHz predicted from the dynamic analysis. This suggests that the analytical model (not described here for brevity) captures the dynamic behavior of the actual fatigue microstructures fairly accurately. It should be pointed out that finite element simulation results confirmed that the in-plane rotation of the microstructures with two and three flexure beams were significantly

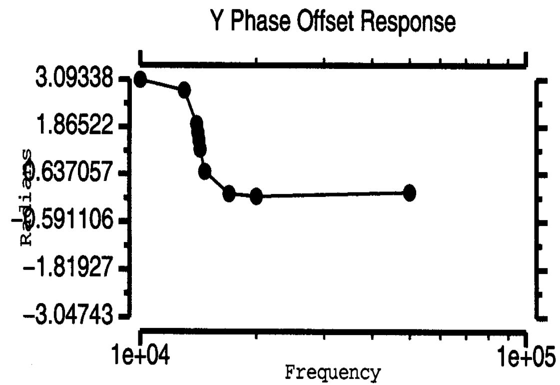

different from those of other fundamental modes. In addition, the electrostatic force used to actuate the specimens is in the plane of motion and the damping for vertical motion of the microdevice is much higher than that for in-plane motion. Thus, actuating the specimens at the desired frequency is fairly straightforward.

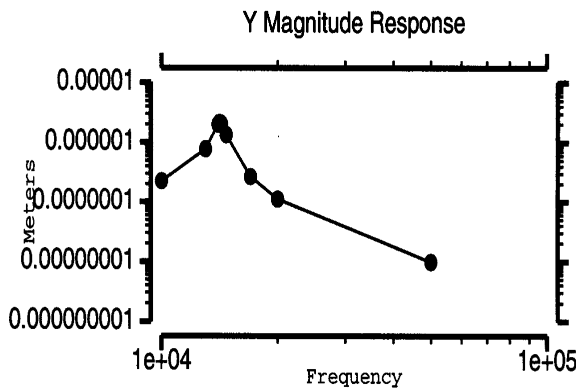

(a) (b)

Figure 3: Frequency response of a fatigue microstructure with two flexure beams of 100 μm length, 2 μm thickness, and 4 μm width: (a) amplitude of in-plane displacement versus frequency and (b) phase shift from the driving force versus frequency.

Figure 4 shows results from short-term fatigue tests performed with different devices having two or three flexure beams of 2 μm thickness, width equal to 2 or 4 μm, and length in the range of 50-90 μm. The microstructures were placed in a multi-probe station and were actuated at resonance by a sinusoidal force

generated by applying a 10 V DC voltage and a 30 V bias voltage at a driving frequency corresponding to the fundamental resonance frequency of the in-plane rotation of the microstructures. In each experiment, the stress amplitude was varied in the range of 0.1-1.0 GPa, but the loading was almost fully reversed, i.e., stress ratio close to –1. However, the stress amplitude was variable since it depends on the device dimensions. All the resonance frequencies of the different specimens are shown to decrease with time, suggesting a reduction in stiffness. Since all the tests were performed in a clean-air laboratory environment under atmospheric conditions and the frequency change is fairly significant, the change in the dynamic response of the devices is attributed to the onset of fatigue damage. Due to the very small dimensions of MEMS, crack initiation mechanisms control the fatigue life. While the mechanism(s) associated with the changes of the dynamic response of the tested microstructures require further investigation, it may be speculated that the observed stiffness degradation is a manifestation of microscopic processes involving intra-/trans-granular microfracture, which cannot be observed macroscopically. It has been reported that subcritical crack growth in polysilicon follows a transgranular path and is due to the synergistic effects of water and stress [11]. The preliminary results shown in Fig. 4 demonstrate the high sensitivity of the present fatigue microstructures to capture extremely small damage levels encountered with the onset of cyclic loading, not pos[illegible]bending specimens.

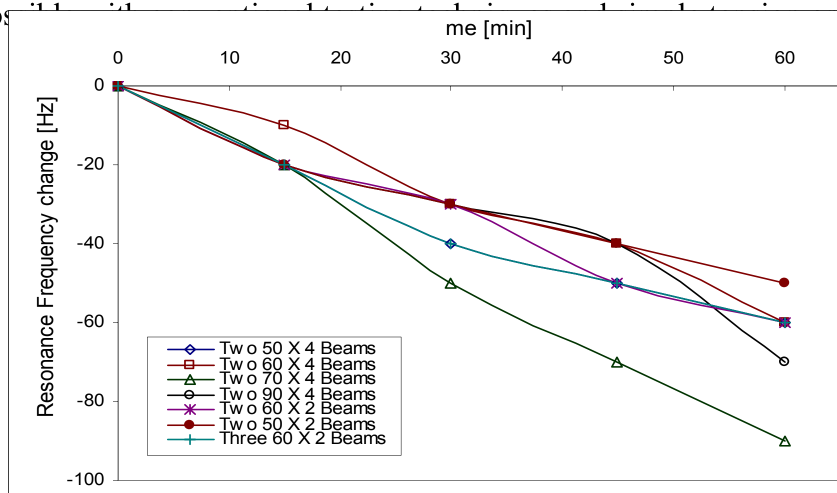

Figure 4. Change of resonant frequency of fatigue microstructures revealing fatigue damage evolution.

CONCLUSIONS

The microfabrication and basic characteristics of MEMS structures for multi-axial fatigue testing were presented along with preliminary results revealing the evolution of fatigue damage. The results demonstrate the feasibility of the adopted testing scheme and the high sensitivity of the microdevices to track small-scale fatigue damage.

ACKNOWLEDGMENTS

This research was supported by the National Science Foundation under Grant No. DMI-9872324 and the Defense Advanced Research Projects Agency/Microelectromechanical Systems (DARPA/MEMS) under Grant No. DABT63-98-1-0011. The author is grateful to P. Stupar and C. Belu for discussions on the design of the specimens and A. Choy and X. Sun for assistance in microfabrication and testing.

REFERENCES

1. Wise, K. D. (1991) *Proc. IEEE Micro Electro Mechanical Systems*, pp. 33-38.

2. Fujita, H. (1997) *Proc. IEEE Micro Electro Mechanical Systems*, pp. 1-8.
3. Greek, S. and Johansson, S. (1997) *Proc. SPIE*, Vol. 3224, pp. 344-351.
4. Sharpe, W. N., Yuan, B., Vaidyanathan, R. and Edwards, B. L. (1997) *Proc. IEEE Micro Electro Mechanical Systems*, pp. 424-429.
5. Koskinen, J., Steinwall, J. E., Soave, R. and Johnson, H. H. (1993) *J. Micromechanics and Microengineering*, Vol. 3, pp. 13-17.
6. Kapels, H., Aigner, R. and Binder, J. (2000) *IEEE Trans. Electron Devices*, Vol. 47, pp. 1522-1528.
7. Kahn, H., Stemmer, S., Nandahumar, K., Heuer, A. H., Mullen, R. L., Ballarini, R. and Huff, M. A. (1996), *Proc. IEEE Micro Electro Mechanical Systems*, pp. 343-348.
8. Tsuchiya, T., Tabata, O., Sakata, J. and Taga, Y. (1997) *Proc. IEEE Micro Electro Mechanical Systems*, pp. 529-534.
9. Jones, P. T., Johnson, G. C. and Howe, R. T. (1996) *Micro Electo Mechanical Systems*, ASME, DSC-Vol. 59, pp. 325-330.
10. Connally, J. A. and Brown, S. B. (1993) *Exper. Mech*. 33, pp. 81-90.
11. Van Arsdell, W. W. and Brown, S. B. (1999) *J. Microelectromechanical Systems*, Vol. 8, pp. 319-327
12. Sun, X., Horowitz, R. and Komvopoulos, K. (2001) *Proc. MEMS Symposium, Int. Mech. Eng. Congress and Exposition*, in press.